Carbon 216 (2024) 118530

Contents lists available at ScienceDirect

Carbon

journal homepage: www.elsevier.com/locate/carbon

Gamma-ray irradiation to achieve high tensile performance of unidirectional CNT yarn laminates

Jin Gyu Park [a,*], Cecil Evers [a], Claire Jolowsky [a], Britannia Vondrasek [b], Kaylee Thagard [a], Michael Czabaj [b], Bailee Ku [a], Yuezhou Wang [c,e], Traian Dumitrică [c,e], Gregory M. Odegard [d], Zhiyong Liang [a]

[a] FAMU-FSU College of Engineering, High-Performance Materials Institute, Florida State University, 2005 Levy Ave., Tallahassee, FL, 32311, USA
[b] Department of Mechanical Engineering, University of Utah, Salt Lake City, UT, 84112, USA
[c] Department of Mechanical Engineering, University of Minnesota, Twin Cities, MN, 55455, USA
[d] Department of Mechanical Engineering, Michigan Technological University, Houghton, MI, 49931, USA
[e] Integrated Engineering, Minnesota State University, Mankato, MN 56001, USA

ARTICLE INFO

Keywords:
Carbon nanotubes
Laminates composite
Gamma-ray irradiation
Carbon nanotube yarn

ABSTRACT

Continuous carbon nanotube (CNT) yarn fabricated from a floating catalyst chemical vapor deposition (FCCVD) method is treated under gamma-ray irradiation to enhance the mechanical properties of the CNT yarn and its unidirectional composite laminates. Gammy-ray doses varying from 50 kGy to 1200 kGy are used to irradiate CNT yarns and their microstructures, tensile properties and surface characterizations are studied. The graphitic structure change is not clear from the transmission electron microscopy, however, the specific tensile strength and modulus of yarn vary slightly within 10 % as the dose increased. This modulus trend coincides with mesoscopic distinct element modeling (mDEM) simulation results. Surface characterization shows additional oxygen functional groups and smaller contact angles after irradiation. Interestingly, the specific tensile properties of composite laminates also increase relative to the yarns, and the unidirectional laminate from CNT yarn treated with the optimal dose of 700 kGy achieves specific strength and modulus as high as 1.89 GPa/gcm^{-3} and 258 GPa/gcm^{-3}, respectively, which are 30.9 % and 37 % increases compared to the control laminate. The results indicate that radiation-induced crosslinking among the CNTs and the formation of surface-active sites leads to enhanced load transfer in the yarns and promote CNT/resin interfacial bonding.

1. Introduction

Carbon nanotubes (CNTs) have high mechanical and electrical properties, which may be used as the primary reinforcement material for high-performance structural composites [1]. Previous methods involved adding CNTs into composites through direct mixing or dispersing them into the resins; however, these methods result in low CNT volume or weight concentrations. Recently, CNT sheets and yarns have been explored for composite fabrication as high concentrations of CNTs (60 vol %) are more easily achieved [2,3]. In addition to the higher concentrations, further alignment of CNT networks was introduced which dramatically improved the mechanical properties of the CNT sheets [4,5] and the resulting composites [3,5,6]. A high degree of alignment of the CNT network, up to 0.92 based on polarized Raman with Gaussian orientation distribution function, was achieved by mechanically stretching sheets of randomly dispersed CNTs, resulting in an ultimate tensile strength over 1.58 GPa and modulus of 252 GPa in composite [5].

Similar to the CNT sheets, CNT yarn and its composite properties also depend on alignment [7], interfacial properties [8], and packing of CNT bundles [9]. CNT yarns can be fabricated through several different methods: direct drawing and densification of CNT socks from a high temperature furnace [10], extruded from liquid crystalline phase of CNTs [11], or drawn from a CNT forest [12]. Each of these methods result in the CNT yarns having high intrinsic alignment critical for high structural performance due to directional stretching or shear interactions between CNTs. This intrinsic alignment of CNT yarns from the fabrication process requires no further processing, in contrast to CNT sheets. However, high alignment results in densely-packed CNT microstructures, which limits the ability of chemical treatments to enhance the interfacial bonding properties between CNT yarn and resin [13].

* Corresponding author.
E-mail address: jgpark@fsu.edu (J.G. Park).

https://doi.org/10.1016/j.carbon.2023.118530
Received 11 July 2023; Received in revised form 5 October 2023; Accepted 14 October 2023
Available online 16 October 2023

Conventional chemical treatments or functionalization techniques may only work on nanotubes at the easily accessible outer surface of CNT yarns. However, e-beam or gamma-ray radiation-induced crosslinks of CNTs could penetrate densely-packed CNT yarn materials. Similar to the polymer radiation treatments [14], subjecting CNT sheets [15,16] and CNT yarns to e-beam or gamma-ray treatments [17–19] has been shown to improve mechanical properties due to possible crosslinks created between the CNTs. However, this treatment may result in damage to the CNT surface walls resulting in decreased properties. For instance, over-dosage of radiation applied on single-walled carbon nanotubes (SWCNTs) was determined to significantly degrade the properties [16]. Numerous studies have been conducted using CNT sheets and yarns as reinforcements [1,3,6,9,20,21], but there is a lack of understanding of the effects of radiation treatment of these materials on laminate-scale composites.

In this study, microstructures, tensile properties and surface characteristics of neat CNT yarns were studied before and after irradiation to determine the effects of gamma-ray treatment at different dosages. Both pristine and treated yarns were used to fabricate unidirectional CNT laminates using scalable filament winding and a hot-press process [22]. The resultant laminates measured 80 mm × 38 mm × 0.2 mm, which allowed for reproducible sample preparation and tensile testing. The tensile properties and failure modes of the composites were investigated to determine the effects of the treatments on mechanical performance and compared with state-of-the-art carbon fiber composites.

2. Materials and methods

MIRALON® high strength 2-ply CSY CNT yarn, manufactured by Nanocomp Technologies, Inc. (now part of Huntsman Advanced Materials), was received for subsequent gamma-ray irradiation. The CNT yarn was synthesized through the floating catalyst chemical vapor deposition (FCCVD) method and proprietary post-treatment process. The resulting yarn has good degree of alignment above 0.7 [22] and very low twist density ~ 0.07 mm^{-1} based on low magnification SEM. Typical linear density of the yarn ranges from 7 to 10 tex (g/km) [22] and corresponding volumetric density is 1.0–1.5 g/cm^3 that is higher than random CNT sheet [13].

Gamma-ray irradiation was conducted at the Radiation Center, Oregon State University, using the Co60 isotope with 1.13 and 1.33 MeV photon energies. The CNT yarns were wrapped around a plastic tube and placed at the center of the irradiation chamber with a uniform irradiation area of 6″ length × 3" diameter. The dose was controlled by the irradiation time. Six different doses were applied: 50 kGy, 100 kGy, 200 kGy, 400 kGy, 700 kGy, and 1200 kGy.

To determine specific strength and modulus, the CNT yarns were tested on Autograph AGS-X (Shimadzu Co.) mechanical test system using TH76-1+Ko (Grip-Engineering Thümler GmbH) capstan grips with 2.5 cm diameter and a 500 N load cell. A gauge length of 120–130 mm was used with a preload of 0.1–0.15 N and stretched until break using 3 N/min loading rate. Strain was calculated by crosshead displacement and a tex (g/km) number measured from a yarn length of 5 ft. Capstan grip provides more proper failure at the gauge region rather than grip area and avoid stress concentration at the clamp exit [23]. More detail experimental procedure of yarn tensile test can be found in ref. [22].

Scanning electron microscopy (SEM) and transmission electron microscopy (TEM) were performed using Helios G4 UC (Thermofisher Scientific) and JEM-ARM200cF (JEOL) instruments, respectively. The TEM cross section of CNT yarn was prepared from lift-out of the lamellae and post-thinning process on the Helios machine, and 80 kV was used for TEM imaging to reduce beam damage.

Raman spectroscopy (785 nm excitation, Invia, Renishaw equipped with a motorized stage) was used to compare the D-band and G-band ratio to investigate molecular damage to the CNTs. Streamlined Raman mapping was performed at 100 % power with a spread beam for fast data acquisition.

Thermogravimetric analysis (TGA) was performed with a Q50 (TA Instruments) under air flow. Temperature dependence of electrical resistivity down to liquid helium temperature was measured using a physical property measurement system (PPMS, Quantum Design). X-ray photoelectron spectroscopy (XPS) was performed in a PerkinElmer PHI-5100 system with Al Kα with X-ray energy of 1486.6 eV. Dynamic contact angle (DCA) was measured using a DCAT15 (Dataphysics), and the sample was advanced into and receded from deionized water at 1 mm/min speed with an immersion depth of 3 mm, which was repeated for 5 cycles. A wetted length was used for DCA calculations based on the measured perimeter of the yarns using an optical microscope.

Unidirectional CNT yarn composite laminates were fabricated using a filament winder as detailed in a previous paper [22]. CYCOM® 5250-4 bismaleimide (BMI) resin (provided by Solvay) was used for the laminate composite fabrication with suggested curing and post-curing cycles. Four laminates were fabricated from 0 kGy (control), 200 kGy, 700 kGy, and 1200 kGy irradiated yarns. The resultant CNT yarn composite laminates were cut to 2–3 mm (W) × 80 mm (L) tensile test coupons and tested with an Instron 5969 load frame equipped with a 50 kN load cell and MTS 646 hydraulic collet grips and tested at 0.3 mm/min. Strain was calculated with an Epsilon One optical extensometer. The modulus was taken via loading, unloading, and reloading cycles over the range from 400 MPa to 1200 MPa.

3. Results and discussion

3.1. Individual CNT yarn results

3.1.1. Molecular structures of CNT yarns

Fig. 1 shows SEM images of CNT yarn surfaces before (Fig. 1 (a)) and after the irradiation treatment of 1200 kGy (Fig. 1 (b)). No observable damage of the CNT bundle structures on the yarn surface was noted, even at the highest dose (1200 kGy). TEM images of the pristine and high-dose treated CNT yarn cross-sections were also acquired to identify any CNT wall damage or internal structure changes from the irradiation. At low magnification (Fig, 1 (c) and (d)), CNT assemblages can be seen with both flattened double-wall CNTs and deformed CNTs as previously reported [5,13]. Even at higher magnifications (Fig. 1 (e) and (f)), clear graphitic structures can be observed. (See additional examples in Fig. S2 in Supplementary Information). Therefore, the radiation effects on the CNTs from TEM image analysis cannot be clearly identified. However, previous research on the gamma-ray irradiation of carbon materials reported different effects on the structural changes for CNT and graphite [24]. In the case of multi-walled CNTs (MWCNTs), some wall damage and graphitic lattice crosslinking were observed along with changes in the Raman spectroscopy and XRD around 200 kGy. The higher dose reduced the defects, and smaller D/G ratio was ascribed to self-healing of dangling bonds. However, graphite was shown to have an opposite tendency [24]. Silambarasan et al. reported an increase of graphitic order at a low dose (below 50 kGy) while a higher dose (over 100 kGy) resulted in distorted graphitic structures [25]. This structural difference with similar doses also originated from a higher dose rate of 5 kGy/h [25], which had more recoiled electrons from Compton scattering. This high dose rate could result in damaged graphitic structures rather than the annealing observed with the low dose rate of 1.87 kGy/h [24]. The dose rate of 3.3 kGy/h used herein was between these two reported rates, which may not result in a monotonic increase of defects, as seen in the higher dose levels.

3.1.2. TGA

Fig. 2 shows the TGA curves and derivatives of the CNT yarns treated at different gamma-ray dosage levels. All curves were from the same yarn batch with similar Fe catalyst residue contents of ~13 wt %. A small amount of weight loss occurred around 300 °C from organic impurities. Two main decomposition peaks occur around 500 °C and

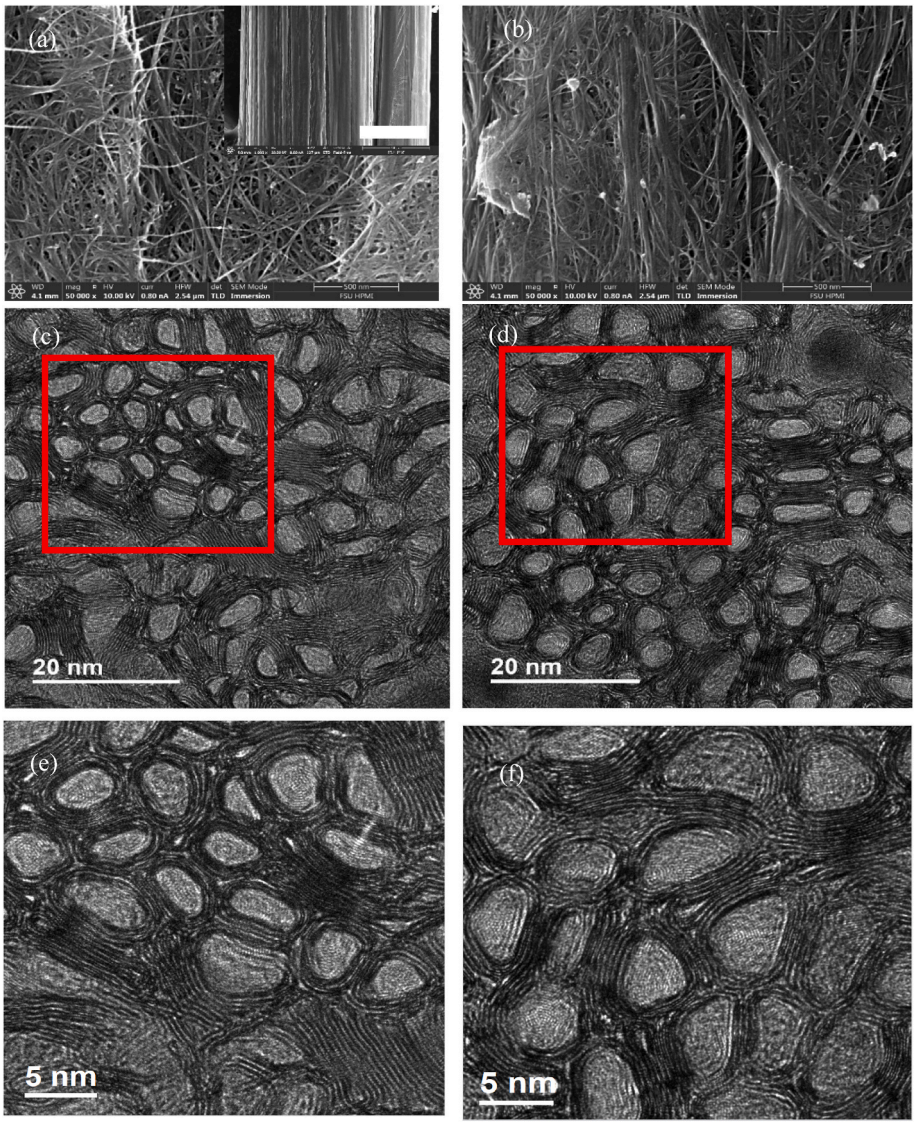

Fig. 1. Microstructures of CNT yarns before and after radiation treatments: (a) SEM image of control CNT yarn as received, inset shows low magnification image of the yarn with a diameter of 120 μm with a scale bar of 40 μm. (b) Surface of CNT yarn after 1200 kGy irradiation, showing CNT bundle network structures. HRTEM images of CNT yarn (c) as received and (d) 1200 kGy irradiated yarns. High magnification image of (e) as received and (f) 1200 kGy irradiated yarn. (A colour version of this figure can be viewed online.)

660–680 °C – the former peak was from either smaller diameter CNTs or amorphous carbon, while the latter was due to double or multi-walled CNTs [26]. The decomposition peak temperature shifted about 36 °C to a lower temperature region (from 684 °C to 648 °C) with the increase in gamma-ray irradiation. This was potentially due to some of the walls of the large diameter double-walled CNTs or MWCNTs (as shown in Fig. 1) becoming slightly damaged during the gamma-ray irradiation, especially in the higher-dosed samples, which thermally decomposed more easily at elevated temperatures. Degradation of thermal stability of graphitic structures has been widely reported in chemical functionalization damaged CNTs [27,28] and electron beam treated carbon fiber (CF) cases as well [29].

3.1.3. *Raman spectra analysis*

Both CNT sheets – either vacuum filtrated SWCNT or CNT sheet from FCCVD - showed smaller D-band intensities (I_D) than the corresponding G-band intensities (I_G), which confirms higher quality with less defects compared to typical MWCNTs with I_D/I_G larger than one [30]. For these high-quality CNT sheets, the D-band intensity ratio (I_D/I_G) increase was clear after gamma-ray irradiation doses up to 1200 kGy (See Supplementary Information, Fig. S3). Contrary to the Raman spectra associated with random CNT orientation and relatively flat surfaces of CNT sheets, Raman spectra of the CNT yarn showed more D/G ratio variations depending on the location due to the highly aligned CNTs, which have a rough surface with curved features, as shown in Fig. 1. Therefore, Raman mapping was performed to observe a large area of the CNT yarn surface and thus obtain more representative results.

The longitudinal direction of the yarn was placed parallel to the laser polarization. Along the longitudinal length of the yarn, there was a higher G-band intensity than in the transverse direction due to the alignment. The D/G ratio was obtained from the integration of the D-band (1200-1400 cm^{-1}) and the G-band (1500-1650 cm^{-1}) peak areas. However, Raman spectroscopy on the surface of the CNT yarn showed some inconsistencies resulting in varied D/G ratios at different locations, as shown in Fig. 3 (a) and (b) for the control and 700 kGy irradiated CNT yarns, respectively. This variation is from the inhomogeneity of the CNT yarn and CNT alignment as seen in SEM. Therefore, the D/G ratio results were averaged among 800–2000 points in each sample. However, the irradiation effects were difficult to identify since the results varied depending on the location measured and between yarn batches, as

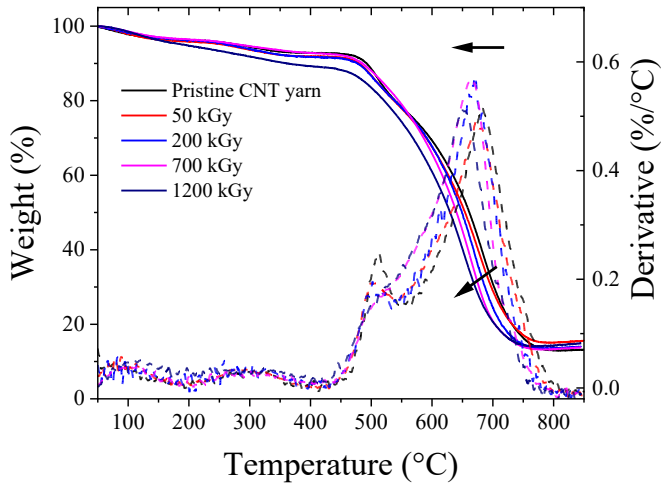

Fig. 2. Weight change and its derivative curves as a function of temperature under air flow. (A colour version of this figure can be viewed online.)

shown in Fig. 3 (c). Compared to the CNT yarn, CNT sheets (either few-wall carbon nanotube from FCCVD process or SWCNT) showed a clear tendency for higher D/G ratios with irradiation treatments. The different D/G ratio trends between the CNT yarns and sheets were due to material structure differences. That is, the CNT yarn was densely packed, while the CNT sheet had many pores in contact with air causing varying degrees of gamma-ray irradiation effectiveness. Oxygen functional groups formed on the surface of CNTs during gamma-ray irradiation [31], and due to the high degree of pores, the CNT sheets had more accessible surface area to allow for reactions. The surface of CNT yarn also has a wrinkled structure with misalignment at some locations, as shown in Fig. 1, which affected the D/G ratio measurements because of its orientation dependence. A similar difference between CNT sheet and irradiated CNT yarn can be observed in the electrical transport measurement as well. CNT yarn with higher degree of alignment shows metallic conductive features as seen in highly doped CNT sheet [32], however, the difference from irradiation is trivial (See Supplementary Information, Fig. S4). Gamma-ray irradiation could damage the CNT structures, yet the crosslinks between the CNTs and oxygen induced surface functional group can increase electrical conductivity as competing factors for improved electrical transport. Thermal conductivity in CNTs is phonon transport dominant [33,34], which could be affected through different irradiation doses.

3.1.4. Tensile properties and failure mode

The tensile properties of the radiation-treated CNT yarns are summarized in Table 1 and plotted in Fig. 4 (typical stress-strain curves are shown in Supplementary Information, Fig. S5). The ultimate breaking forces increased with higher doses, but the specific strength values showed a slight increment and reduction trend due to the tex (g/km) value changes after gamma-ray irradiation. This increase of tex values at higher doses could be related to the radiation induced surface modification during the irradiation in open air. Similar increase and decrease in the specific modulus of the CNT yarns also occurred as the irradiation dose increased. For carbon materials, irradiation leads to an increase of the surface functional groups and an increase of oxygen concentration. In the pristine carbon fiber [35,36] or activated carbon [37], the weight increase could be due to this oxygen related additional functional groups. Additionally, the gamma-ray irradiated MWCNTs tend to be easily functionalized via a chemical functionalization compared to pristine MWCNTs [38]. Previous research of CNT yarns drawn from a MWCNT forest by a CVD process also showed similar trends for the strength and modulus increases upon irradiation in air, up to 600 kGy [31]. Increased oxygen concentrations on CNTs, with the advantage of a densely packed CNT networks, resulted in higher property improvements due to the possible crosslinks between CNTs [31]. Therefore, irradiation could increase the density of functionalization groups on the CNT yarn surface and result in mechanical property enhancement through crosslinks among nanotubes or organic impurities.

Fig. 5 shows SEM images of the 200 kGy treated CNT yarn fracture after capstan grip tensile testing. This yarn showed the highest specific strength among the irradiated CNT yarns, as shown in Fig. 4. However, all other CNT yarns exhibited a similar fracture behavior, where the bundles failed through pull-out failure of the bundles (See Supplementary Fig. S6), which is similar to the untreated yarn failures [7].

3.1.5. Modeling of tensile properties CNT bundles after radiation-induced defects

Using the tools of density-functional theory tight-binding DFTB [39] and mesoscopic distinct element modeling (mDEM) [40], shown in Fig. 6, we derived a deeper understanding on the structures and processes responsible for the observed change in mechanical properties of the yarns subjected to various irradiation dosages. Atoms knocked from the CNT lattice by irradiation produce both vacancies and shared covalent bonds in graphitic layers. Starting with the di-vacancy defect structure V2 in a graphene bi-layer proposed by Telling et al. [41], we constructed larger-vacancy structures, such as V14 and V28, which are associated with an increased irradiation dosage, shown in Fig. 6(a). While these defects comprise nanoholes on opposite faces, they still covalently bridge the graphene van der Waals contacts at the undisturbed 3.34 Å interlayer distance. Their structural features impact the mesoscale mechanics of CNTs in opposing ways, represented by mDEM

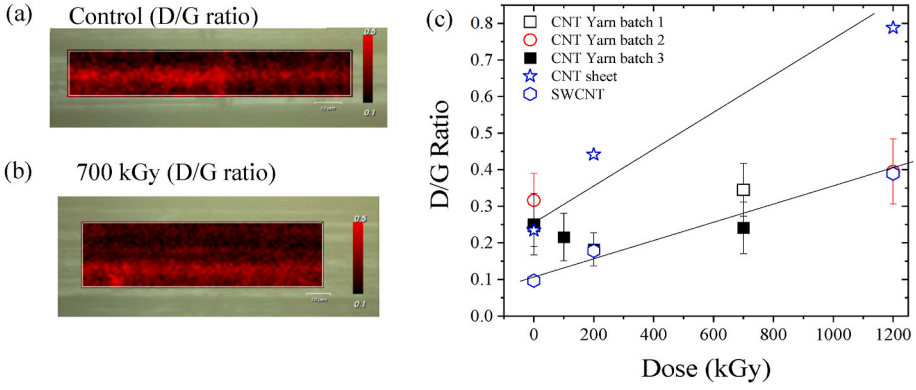

Fig. 3. Raman mapping of D/G ratio by peak area from (a) control CNT yarn and (b) 700 kGy dose with same color scale up to $I_D/I_G = 0.5$. Variations in measurements depended on the location. (c) D/G ratio with different gamma-ray doses for different CNT yarn and sheets. The CNT sheet has a monotonic increase (linear line for guiding eyes) of the D-band with higher doses compared to the fluctuation in CNT yarns. (A colour version of this figure can be viewed online.)

Table 1
Summary of single CNT yarn mechanical properties after gamma-ray irradiation.

Sample Dose (KGy)	Tex (g/km)	Force (N)	Increase (%)	Specific Strength (N/tex)	Increase (%)	Specific Modulus (N/tex)	Increase (%)
0	7.57	13.4 ± 0.5		1.77 ± 0.07		92.6 ± 3.2	
50	7.49	13.6 ± 0.5	+1.5	1.82 ± 0.07	+2.8	89.7 ± 3.8	−3.1
100	7.48	13.8 ± 1.0	+3.0	1.84 ± 0.07	+4.0	95.7 ± 1.5	3.3
200	7.48	13.8 ± 0.9	+3.0	1.85 ± 0.12	+4.5	97.2 ± 1.8	5
700	8.27	14.3 ± 0.3	+6.7	1.73 ± 0.04	−2.3	87.0 ± 0.7	−6.0
1200	8.48	14.7 ± 0.2	+9.7	1.73 ± 0.02	−2.3	83.5 ± 3.1	−9.8

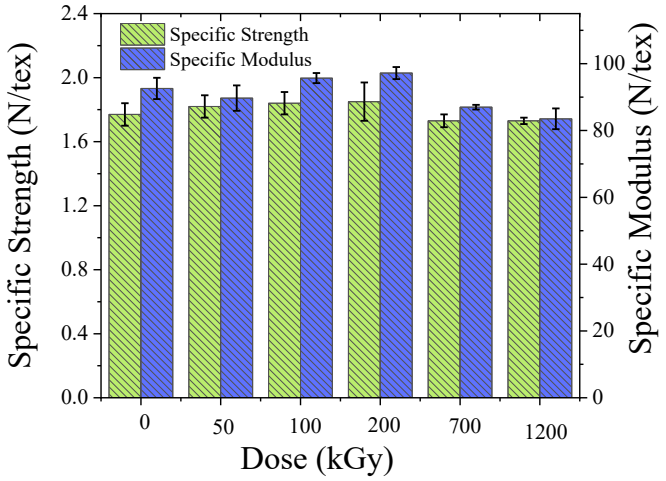

Fig. 4. Tensile properties of the CNT yarns. Specific strength and modulus of individual CNT yarn with different dose levels of gamma-ray irradiation. (A colour version of this figure can be viewed online.)

in Fig. 6(b). While the strong covalent crosslinks provide enhanced shear interfaces (k_s) at the otherwise weak van der Waals CNT contacts [42], the associated nanoholes weaken locally the in-plane CNT elasticity, captured in mDEM through the spring constants, k_n. We used the method of Ostanin et al. [40] to provide DFTB data for a mDEM model for a 40 nm long bundle [43] consisting of 19 CNTs with discontinuities and vacancy-cross-link defects. The computed Young's modulus of this bundle, Fig. 6 (c), displays non-monotonic variations with the number of defects. The initial Young's modulus increase indicates a dominant contribution of the k_s shear interfaces, which enhance the load transfer between CNTs. The modulus decrease at the larger number of defects reflects instead the detrimental effects of lowering k_n by larger nanoholes. As the macroscopic yarn comprises a complex structure of interwined bundles [44], we infer that the observed maximization of the Young's modulus under the 200 kGy dosage reflects the balancing act of the shear interface strengthening and CNT weakening introduced by irradiation-induced atomistic-scale vacancy-cross-linking defects.

3.1.6. *Characterization of modified CNT yarn surface*

Fig. 7 shows the C1s XPS of the CNT yarn before and after gamma-ray irradiation. Compared to the control sample, a slight increase of the C–O/O–C–O related peak occurred around 286.5 eV, and the O–C═O peak happened around 288.3 eV. This change was similar to commonly observed CNT surfaces from acid-treated CNT sheets where the surface modification enhanced the interfacial bonding between CNTs and resin, resulting in greater mechanical properties [44,45]. Table 2 shows the XPS survey, including C and O only, and results of each CNT yarn after irradiation. The yarns were from different manufacturing batches, and the control sample had a C–O related bonding with high amounts of oxygen, likely due to organic impurities in the CNT yarn formed during the fabrication process, as observed in the TGA curves. The increase of the O–C═O and C–O bonding was seen after the gamma-ray irradiation, which agrees with previous reports [31].

Surface modification can also be observed from the contact angle measurements. Contact angles were evaluated via a static droplet method by measuring the angle between the material and tangent of the liquid drop (See Supplementary Information, Fig. S7 and Table S1). However, this static angle can only be used to determine the initial contact between the material and the liquid and does not measure the material properties after the material has been wet-out with the liquid. Additionally, the irregular surfaces of the current CNT yarns also pose a challenge to accurately measure contact angles. DCA could solve these issues by measuring both the initial material interaction with the liquid and continuing to measure the interaction as the material is advanced into, and recedes from, the working liquid.

The wetting properties of deionized water on CNT yarn were measured before and after different irradiation doses, which were then used for yarn laminate fabrication. Table 3 shows the comparison of the wetting angle before and after the irradiation. Interestingly, the contact angle reduced after irradiation, and the reduction had the greatest difference in the case of 700 kGy. However, the lowest contact angle was seen in the 1200 kGy treated yarns (See Supplementary Information, Fig. S8 for DCA measurement of 700 kGy). The drastic contact angle decreasing in the 1200 kGy treatment may indicate over-processing of the yarns with more defects, which resulted in the lower mechanical properties that were seen in the composite laminates. This is another indication of the effectiveness of the modification of the yarn surface via the radiation treatment.

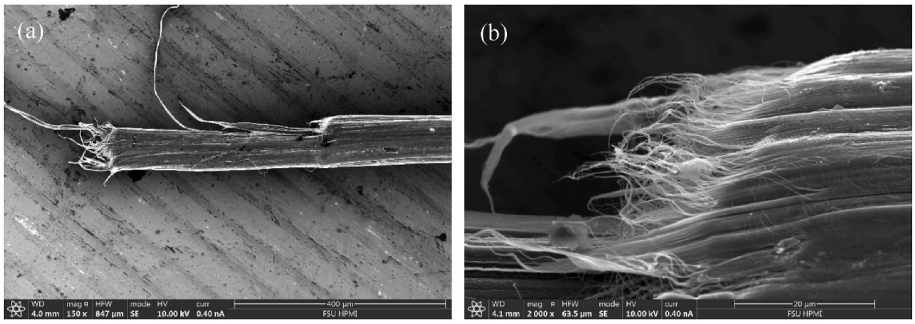

Fig. 5. Fracture surface of the 200 kGy treated yarn (a) typical fracture area image of gamma-ray treated CNT yarn; (b) pull-out failure mode of CNT bundles can be seen clearly. (A colour version of this figure can be viewed online.)

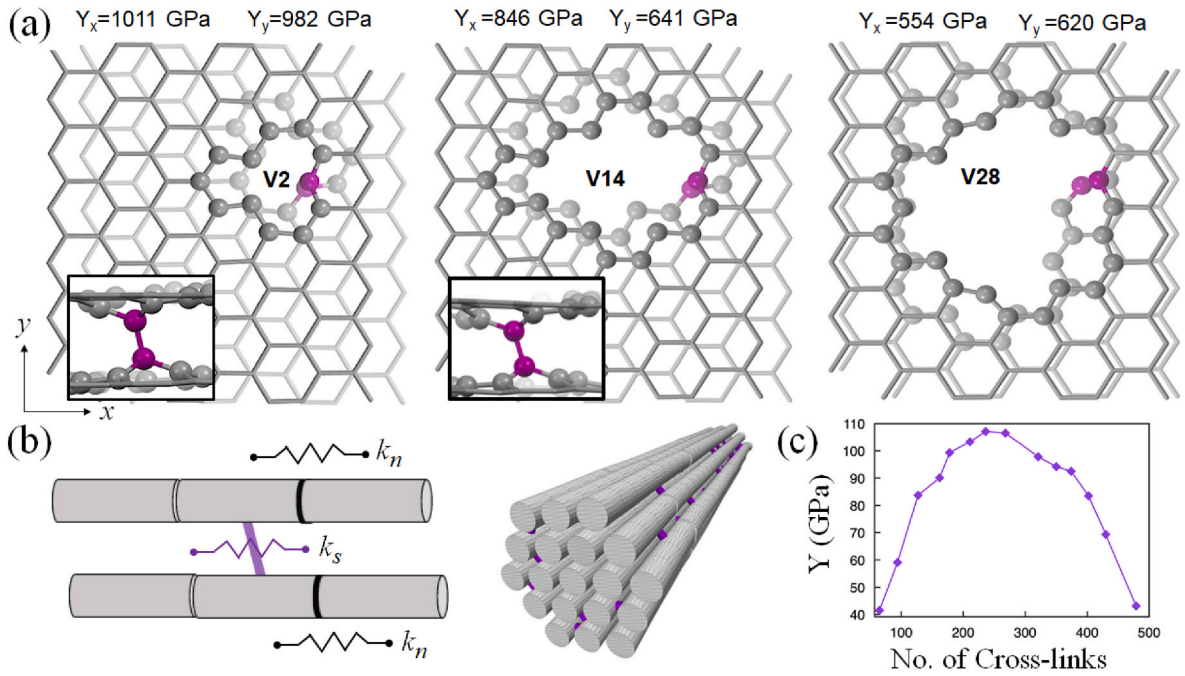

Fig. 6. (a) DFTB-computed models of cross-links (purple atoms) bridging holey graphitic bi-layers with various numbers of vacancies (V): V2 (left), V14 (center), and V28 (right). The in-plane Young's moduli provided above each structure. Inset is the side view of the cross-link. (b) Distinct element (gray cylinders) representation of two cross-linked CNT portions, with the elasticity of the cross-link and perforated wall captured by atomistical-informed shear ks and linear kn springs (left); a 40 nm long bundle with CNT discontinuities and cross-links. (right) (c) mDEM computation of the Young's modulus of the bundle vs. number of cross-links. (A colour version of this figure can be viewed online.)

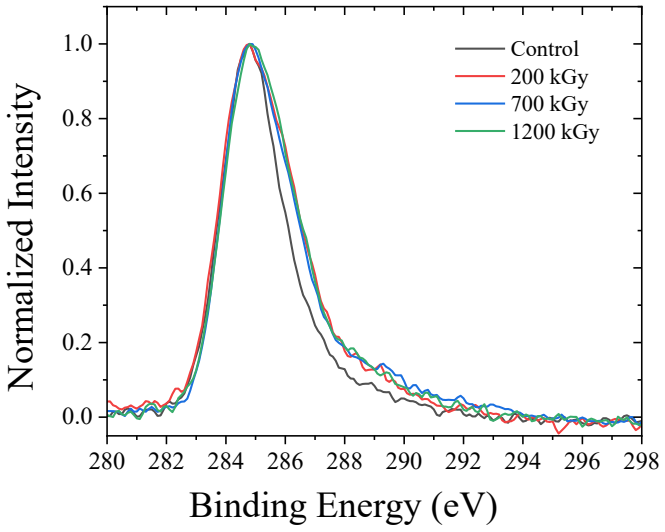

Fig. 7. C1s XPS with different gamma-ray dose. Increased O–C=O bonding related peak shows the surface modification of CNTs with oxygen in the air during the irradiation. (A colour version of this figure can be viewed online.)

Table 2
Increase of the oxygen containing groups with gamma-ray irradiation.

Atomic %	Survey At. %		C–C	C–O	O–C=O
	C	O	284.5-8eV	286.3–5 eV	288.1–3 eV
Control	86.85	13.15	74.0 %	16.2 %	10.0 %
200 kGy	88.45	11.55	67.1 %	19.8 %	13.1 %
700 kGy	88.32	11.68	70.4 %	11.3 %	18.3 %
1200 kGy	87.95	12.05	66.0 %	17.3 %	16.7 %

In general, the advancing contact angle ($\theta_{D,a}$) is larger than receding contact angle ($\theta_{D,r}$), and the static contact angle (θ_S) is in between those two values [46]. Control samples of each yarn batch exhibited an average contact angle of 70° with some variations; however, the decrease in contact angle after gamma-ray exposure was clear for all CNT yarn samples except for a slight increase with the 200 kGy dose. For CF, increased C–O bonding, shown by XPS, increased the hydrophilic percentage and reduced the contact angle accordingly [47]. Similarly, oxygen plasma treatment of a CNT mat also significantly reduced the contact angle by increasing C–O bonding [48]. In this study, the CNT yarn contact angles were slightly smaller than other CNT fibers drawn from CVD-grown MWCNTs with equilibrium values around 90° [49], and the difference between advancing and receding angles were smaller. These behaviors may be due to densely-packed CNT structures without any air gaps and some polarized impurities on the surface.

3.2. Tensile properties of unidirectional CNT yarn composite laminates

The gamma-ray irradiated CNT yarns with three different dose levels (200 kGy, 700 kGy and 1200 kGy) were selected for unidirectional CNT composite laminate fabrication (See Supplementary Information, Figs. S9 and S10). All of the control and gamma-ray irradiated samples showed densely-packed CNT yarn microstructures, (See Supplementary Information, Fig. S11), which confirmed the composite laminate fabrication process consistently produced quality results.

Tensile properties of the gamma-ray irradiated CNT yarn/BMI resin matrix laminates, along with a control sample, were measured (Table 4). See Supplementary Information for procedure details. Fig. 8 (a) shows the specific modulus and strength of unidirectional CNT yarn composite laminates. CNT yarn and its laminate film have similar specific strengths, because the dominant properties are from CNT yarn and low resin contents in the laminate. However, the modulus is much higher in the laminate film due to additional pressing and adhesion among yarns. A significant enhancement over 30 % was observed for both specific modulus and strength. For the individual CNT yarns, the modulus

Table 3
Dynamic contact angle measurement of CNT yarn with water used in the laminate manufacturing.

		200 kGy		700 kGy		1200 kGy	
		Dynamic	Avg.	Dynamic	Avg.	Dynamic	Avg.
Control	$\theta_{D,a}$	86.03°	72.47° ± 4.02	86.88°	74.47° ± 4.55	78.67°	62.50° ± 8.70
	$\theta_{D,r}$	58.90°		62.07°		46.33°	
Irradiated	$\theta_{D,a}$	84.72°	70.17° ± 4.27	80.04°	64.36° ± 5.15	73.71°	54.12° ± 9.93
	$\theta_{D,r}$	55.60°		48.68°		34.54°	

Table 4
Mechanical properties of unidirectional laminates using gamma-ray irradiated CNT yarns.

Unidirectional CNT yarn/BMI laminates	Specific Modulus (GPa/g cm^{-3})	% Increase	Specific Strength (GPa/g cm^{-3})	% Increase
Control	197 ± 33	–	1.38 ± 0.10	–
200 kGy	228 ± 41	15.7 %	1.64 ± 0.08	18.8 %
700 kGy	258 ± 25	30.9 %	1.89 ± 0.11	37.0 %
1200 kGy	210 ± 12	6.6 %	1.54 ± 0.06	11.6 %

improvement, as shown in Fig. 4, was as high as 5 %, and the specific strength improvement was minimal (<10 %). However, in the unidirectional composite laminates, the specific strength properties of the laminates with 200 kGy and 700 kGy treated yarns demonstrated noticeable increases of over 15 % and 30 %, respectively. The specific modulus also increased by a similar amount of 18.8 % and 37 %, respectively. Laminate films demonstrated significant dose dependent improvements compared to yarn. Therefore, the gamma-ray treatment could result in more effective load transfer in the composite due to the surface modifications, as shown by the XPS and contact angle results and in previous research [19]. Similarly, a gamma-ray irradiated CF composite was also shown to exhibit a higher flexural modulus and strength than the pristine fiber composite [36]. Furthermore, the 700 kGy CNT yarn had a low contact angle and showed the greatest difference compared to its yarn control, which led to the best composite property enhancements compared to the control laminate.

The 1200 kGy dose treatment decreased the mechanical properties compared to the 200 and 700 kGy dose cases and exhibited only slight property improvements compared to the control laminate. This could be an indication of excessive structural damage to the CNT walls that compromises their load-carrying capacity with higher irradiation doses. Fig. 8 (b) shows an Ashby chart of specific modulus vs specific strength with the state-of-the-art unidirectional CF composites, aerospace metal alloys, and the unidirectional CNT yarn laminates discussed herein. The composite laminate with the 700 kGy treated yarns shows a unique combination of higher specific strength and modulus, which is not available from the M60J, IM7 and T1100G unidirectional carbon fiber composites. (see Supplementary Information, Table S2 for more detailed composite property information).

Fig. 9 shows typical SEM images of fracture areas of the control and gamma-ray irradiated CNT yarn laminates. Fig. 9 (a) is a low-magnification fracture area, where yarn fractures appear to occur at different locations. Both the control and gamma-ray irradiated laminates exhibit the peeling of ribbons (CNT bundles) from the CNT yarns, as shown in Fig. 9 (b). CNT bundles peeled from the yarn surfaces indicate good interaction, load transfer between yarns, and the existence of resin between the yarns. Each CNT yarn fracture in Fig. 9 (c) and (d) from the 200 kGy laminate shows a similar fracture image as the individual CNT yarn fracture in Fig. 5, that is, the failed CNT bundles exhibited a triangular microstructure on the fracture surface.

Fig. 10 (a) shows the Raman mapping of the cross-section of the CNT yarns in a composite laminate using a 785 nm excitation laser. The Raman map for each CNT yarn cross section contained between 800 and 2000 points of spectra, and the D/G areal ratio was obtained as used in Fig. 3. There were some D/G ratio variations that were dependent on the location measured, CNT orientation, and the presence of resin or organic impurities, as previously discussed. Mapping a larger area over 30 × 20 μm could remove these artifacts and provide more representative results than single or several points measurement. As shown in Fig. 10 (b), increases in gamma-ray irradiation dosage resulted in increases in the D-band intensity, as expected. However, the D/G ratio decreased for the 1200 kGy composite, which may be related to the decreased mechanical properties of the composite at the same dose. Since CNT alignment in the yarn is not parallel to the laser polarization, as shown in Fig. 3, the G-band intensity from tangential mode was smaller, resulting in a higher

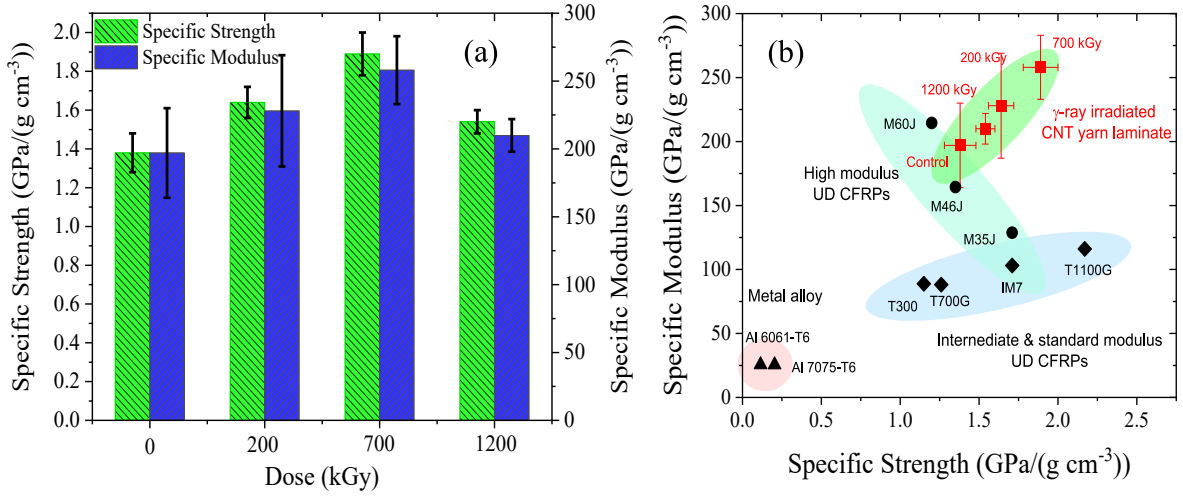

Fig. 8. (a) Specific tensile strength and modulus of unidirectional CNT yarn composite fabricated with different doses of gamma-ray irradiation. (b) Comparison of unidirectional gamma-ray irradiated CNT yarn composites with unidirectional CF composites (60 vol % fiber volume fraction) and metal alloys [22]. (A colour version of this figure can be viewed online.)

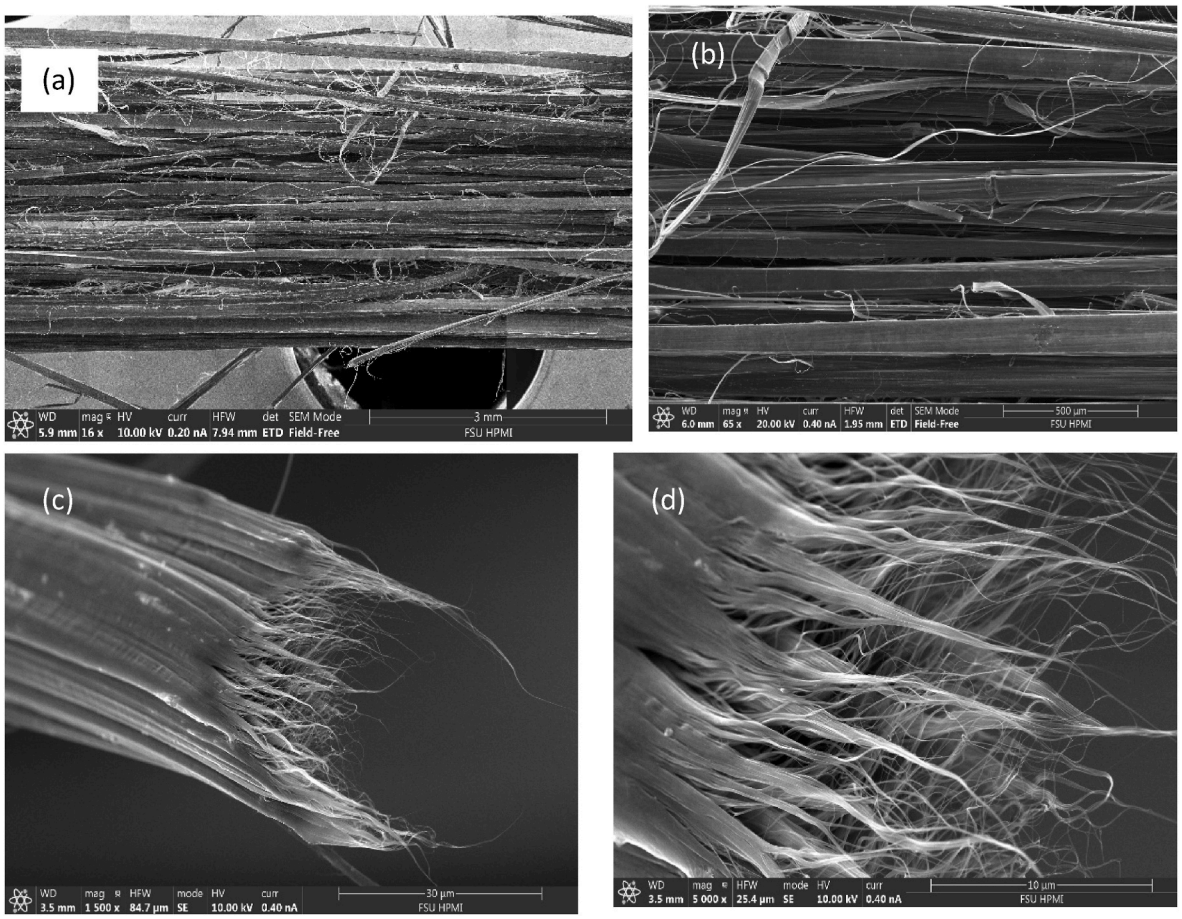

Fig. 9. SEM images of typical fracture area from the unidirectional CNT yarn composite laminates (200 kGy): (a) Low magnification of CNT yarn laminate fracture. (b) Delamination of CNT bundles from the yarn surface. (c)(d) High magnification for individual CNT yarn fractures which shows triangular shape pull out similar to the single CNT yarn fracture. (A colour version of this figure can be viewed online.)

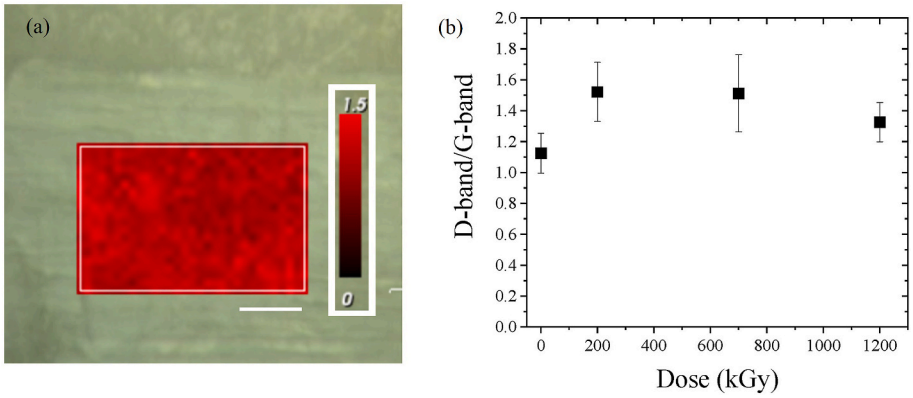

Fig. 10. (a) Raman mapping of D-band/G-band areal ratio using 785 nm excitation overlapped with an optical image of the cross section of the control laminate (CNT yarn area). The scale bar is 10 μm. (b) Summary of results with different dose levels. (A colour version of this figure can be viewed online.)

D/G ratio. Additional research is needed to understand the mechanisms of the D/G ratio decrease observed at higher doses.

4. Conclusion

Gamma-ray irradiation to the CNT yarn improved the specific tensile modulus of yarn, and the resultant unidirectional yarn laminates showed an increase of both specific tensile modulus and strength. The highest tensile properties of the composite laminates were obtained from the CNT yarn with a 700 kGy dose treatment and this modulus maximum coincides with mDEM simulation results. An increase in the yarn linear density in conjunction with XPS results indicate successful surface modification resulting in increased oxygen-containing groups. As a result, this surface modification improved wettability and interfacial bonding between CNT yarn and the resin matrix. Therefore, the specific modulus and strength of the resultant unidirectional CNT yarn composite was improved up to 258 GPa/gcm^{-3} and 1.89 GPa/gcm^{-3}, respectively. This combination of high specific tensile strength and

modulus surpasses a major limit of tensile performance of either high modulus or high strength state-of-the-art unidirectional CF composites. Additionally, over 300 m of CNT yarn treatments and manufacturing performed are scalable for larger size composites. The results show that radiation functionalization has good scalability to support composite laminate fabrication using high-strength CNT yarns. The higher mechanical properties capable of scalability enhance the CNT laminates use for potential aerospace structural applications.

CRediT authorship contribution statement

Jin Gyu Park: Writing – original draft, Writing – review & editing, Investigation, Data curation, Visualization, Supervision. **Cecil Evers:** Investigation, Visualization, Methodology, Writing – original draft. **Claire Jolowsky:** Investigation, Writing – original draft. **Britannia Vondrasek:** Investigation, Methodology, Visualization. **Kaylee Thagard:** Investigation. **Michael Czabaj:** Methodology, Project administration. **Bailee Ku:** Investigation. **Yuezhou Wang:** Software, Formal analysis, Visualization. **Traian Dumitrică:** Software, Formal analysis, Writing – original draft. **Gregory M. Odegard:** Funding acquisition, Project administration, Writing – review & editing. **Zhiyong Liang:** Conceptualization, Funding acquisition, Supervision, Project administration, Writing – review & editing.

Declaration of competing interest

The authors declare that they have no known competing financial interests or personal relationships that could have appeared to influence the work reported in this paper.

Acknowledgements

This work was supported by the Institute for Ultra-Strong Composites by Computational Design (US-COMP, NASA NNX17AJ32G, a NASA Space Technology Research Institute (STRI)). We would like to thank Dr. Emilie Siochi and the NASA Structural CNT Development team for their support and guidance. TEM work was performed at the National High Magnetic Field Laboratory, which is supported by National Science Foundation Cooperative Agreement No. DMR-1644779 and the State of Florida. We also would like to thank Cytec/Solvay and Huntsman for providing nanotube yarn and resin matrix support as well as guidance. We appreciate the support of the Solvay Doctorial Fellowship. Finally, we would like to thank Mr. Jerry Horne for offering his expertise in composite manufacturing processes.

Appendix A. Supplementary data

Supplementary data to this article can be found online at https://doi.org/10.1016/j.carbon.2023.118530.

References

[1] N.P. Singh, V.K. Gupta, A.P. Singh, Graphene and carbon nanotube reinforced epoxy nanocomposites: a review, Polymer 180 (2019), 121724, https://doi.org/10.1016/j.polymer.2019.121724.
[2] Z. Wang, Z. Liang, B. Wang, C. Zhang, L. Kramer, Processing and property investigation of single-walled carbon nanotube (SWNT) buckypaper/epoxy resin matrix nanocomposites, Compos Part A Appl Sci Manuf 35 (2004) 1225–1232, https://doi.org/10.1016/j.compositesa.2003.09.029.
[3] Q. Cheng, J. Bao, J.G. Park, Z. Liang, C. Zhang, B. Wang, High mechanical performance composite conductor: multi-walled carbon nanotube sheet/bismaleimide nanocomposites, Adv. Funct. Mater. 19 (2009) 3219–3225, https://doi.org/10.1002/adfm.200900663.
[4] J.G. Park, J. Smithyman, C.Y. Lin, A. Cooke, A.W. Kismarahardja, S. Li, R. Liang, J. S. Brooks, C. Zhang, B. Wang, Effects of surfactants and alignment on the physical properties of single-walled carbon nanotube buckypaper, J. Appl. Phys. 106 (2009), 104310, https://doi.org/10.1063/1.3255901.
[5] C. Jolowsky, R. Sweat, J.G. Park, A. Hao, R. Liang, Microstructure evolution and self-assembling of CNT networks during mechanical stretching and mechanical properties of highly aligned CNT composites, Compos. Sci. Technol. 166 (2018) 125–130, https://doi.org/10.1016/j.compscitech.2018.04.003.
[6] A. Mikhalchan, T. Gspann, A. Windle, Aligned carbon nanotube–epoxy composites: the effect of nanotube organization on strength, stiffness, and toughness, J. Mater. Sci. 51 (2016) 10005–10025, https://doi.org/10.1007/s10853-016-0228-6.
[7] Y.-S. Dessureault, C. Jolowsky, S. Bell, S. Spiric, J. Molyneux, J.G. Park, A. Hao, Z. Liang, Tensile performance and failure modes of continuous carbon nanotube yarns for composite applications, Mater. Sci. Eng., A 792 (2020), 139824, https://doi.org/10.1016/j.msea.2020.139824.
[8] S. Zhang, A. Hao, N. Nguyen, A. Oluwalowo, Z. Liu, Y. Dessureault, J.G. Park, R. Liang, Carbon nanotube/carbon composite fiber with improved strength and electrical conductivity via interface engineering, Carbon 144 (2019) 628–638, https://doi.org/10.1016/j.carbon.2018.12.091.
[9] X. Wei, J. Wang, H. Ma, F.I. Farha, S. Bi, Q. Zhang, F. Xu, Super-strong CNT composite yarn with tight CNT packing via a compress-stretch process, Nanoscale 14 (2022), https://doi.org/10.1039/d2nr00874b, 9078.
[10] Y.L. Li, I.A. Kinloch, A.H. Windle, Direct spinning of carbon nanotube fibers from chemical vapor deposition synthesis, Science 304 (2004) 276–278, https://doi.org/10.1126/science.1094982.
[11] N. Behabtu, C.C. Young, D.E. Tsentalovich, O. Kleinerman, X. Wang, A.W.K. Ma, E. Amram Bengio, R.F. ter Waarbeek, J.J. de Jong, R.E. Hoogerwerf, S.B. Fairchild, J.B. Ferguson, B. Maruyama, J. Kono, Y. Talmon, Y. Cohen, M.J. Otto, M. Pasquali, Strong, light, multifunctional fibers of carbon nanotubes with ultrahigh conductivity, Science 339 (2013) 182–186, https://doi.org/10.1126/science.1228061.
[12] M. Zhang, K. Atkinson, R. Baughman, Multifunctional carbon nanotube yarns by downsizing an ancient Technology, Science 306 (2004) 1358–1361, https://doi.org/10.1126/science.1104276.
[13] R.D. Downes, A. Hao, J.G. Park, Y.F. Su, R. Liang, B.D. Jensen, E.J. Siochi, K. E. Wise, Geometrically constrained self-assembly and crystal packing of flattened and aligned carbon nanotubes, Carbon 93 (2015) 953–966, https://doi.org/10.1016/j.carbon.2015.06.012.
[14] A.T. Naikwadi, B.K. Sharma, K.D. Bhatt, P.A. Mahanwar, Gamma radiation processed polymeric materials for high performance applications: a review, Front. Chem. 10 (2022), https://doi.org/10.3389/fchem.2022.837111.
[15] S. Wang, Z. Liang, B. Wang, C. Zhang, High-strength and multifunctional macroscopic fabric of single-walled carbon nanotubes, Adv. Mater. 19 (2007) 1257–1261, https://doi.org/10.1002/adma.200602140.
[16] V. Skákalová, Effect of Gamma-Irradiation on Single-Wall Carbon Nanotube Paper, AIP Publishing, 2003, pp. 143–147, https://doi.org/10.1063/1.1628005.
[17] S.G. Miller, T.S. Williams, J.S. Baker, F. Solá, M. Lebron-Colon, L.S. McCorkle, N. G. Wilmoth, J. Gaier, M. Chen, M.A. Meador, Increased tensile strength of carbon nanotube yarns and sheets through chemical modification and electron beam irradiation, ACS Appl. Mater. Interfaces 6 (2014) 6120–6126, https://doi.org/10.1021/am4058277.
[18] M.C. Evora, N. Hiremath, X. Lu, N.G. Kang, L.G. De Andradae Silva, G. Bhat, J. Mays, Effect of electron beam and gamma rays on carbon nanotube yarn structure, Mater. Res. 20 (suppl 2) (2017) 386–392, https://doi.org/10.1590/1980-5373-mr-2017-0102.
[19] J.Y. Cai, J. Min, M. Miao, J.S. Church, J. McDonnell, R. Knott, S. Hawkins, C. Huynh, Enhanced mechanical performance of CNT/Polymer composite yarns by γ-irradiation, Fibers Polym. 15 (2014) 322–325, https://doi.org/10.1007/s12221-014-0322-9.
[20] A.E. Bogdanovich, P.D. Bradford, Carbon nanotube yarn and 3-D braid composites. Part I: tensile testing and mechanical properties analysis, Compos. Appl. Sci. Manuf. 41 (2010) 230–237, https://doi.org/10.1016/j.compositesa.2009.10.002.
[21] J.C. Long, H. Zhan, G. Wu, Y. Zhang, J.N. Wang, High-strength carbon nanotube/epoxy resin composite film from a controllable cross-linking reaction, Compos. Appl. Sci. Manuf. 146 (2021), 106409, https://doi.org/10.1016/j.compositesa.2021.106409.
[22] C.E. Evers, B. Vondrasek, C.N. Jolowsky, J.G. Park, M.W. Czabaj, B.E. Ku, K. R. Thagard, G.M. Odegard, Z. Liang, Scalable high tensile modulus composite laminates using continuous carbon nanotube yarns for aerospace applications, ACS Appl. Nano Mater. 6 (2023) 11260–11268, https://doi.org/10.1021/acsanm.3c01266.
[23] T.S. Gspann, N.H.H. Ngern, P.J. Kiley, P.A. McKeown, J.S. Bulmer, A.H. Windle, V. B.C. Tan, J.A. Elliott, A comparative study of the tensile failure of carbon nanotube, Dyneema and carbon fibre tows over six orders of strain rate, Carbon 164 (2020) 407–421, https://doi.org/10.1016/j.carbon.2020.03.051.
[24] B. Li, Y. Feng, K. Ding, G. Qian, X. Zhang, J. Zhang, The effect of gamma ray irradiation on the structure of graphite and multi-walled carbon nanotubes, Carbon 60 (2013) 186–192, https://doi.org/10.1016/j.carbon.2013.04.012.
[25] D. Silambarasan, V.J. Surya, K. Iyakutti, K. Asokan, V. Vasu, Y. Kawazoe, Gamma (γ)-ray irradiated multi-walled carbon nanotubes (MWCNTs) for hydrogen storage, Appl. Surf. Sci. 418 (2017) 49–55, https://doi.org/10.1016/j.apsusc.2017.02.262.
[26] E. Mansfield, A. Kar, S.A. Hooker, Applications of TGA in quality control of SWCNTs, Anal. Bioanal. Chem. 396 (2010) 1071–1077, https://doi.org/10.1007/s00216-009-3319-2.
[27] L. Thi Mai Hoa, Characterization of multi-walled carbon nanotubes functionalized by a mixture of HNO_3/H_2SO_4, Diam. Relat. Mater. 89 (2018) 43–51, https://doi.org/10.1016/j.diamond.2018.08.008.
[28] Z. Zhao, Z. Yang, Y. Hu, J. Li, X. Fan, Multiple functionalization of multi-walled carbon nanotubes with carboxyl and amino groups, Appl. Surf. Sci. 276 (2013) 476–481, https://doi.org/10.1016/j.apsusc.2013.03.119.

[29] M.S. Park, Y. Ko, M.J. Jung, Y.S. Lee, Stabilization of pitch-based carbon fibers accompanying electron beam irradiation and their mechanical properties, Carbon Letters 16 (2015) 121–126, https://doi.org/10.5714/CL.2015.16.2.121.
[30] P. Delhaes, M. Couzi, M. Trinquecoste, J. Dentzer, H. Hamidou, C. Vix-Guterl, A comparison between Raman spectroscopy and surface characterizations of multiwall carbon nanotubes, Carbon 44 (2006) 3005–3013, https://doi.org/10.1016/j.carbon.2006.05.021.
[31] M. Miao, S.C. Hawkins, J.Y. Cai, T.R. Gengenbach, R. Knott, C.P. Huynh, Effect of gamma-irradiation on the mechanical properties of carbon nanotube yarns, Carbon 49 (2011) 4940–4947, https://doi.org/10.1016/j.carbon.2011.07.026.
[32] S. Zhang, J.G. Park, N. Nguyen, C. Jolowsky, A. Hao, R. Liang, Ultra-high conductivity and metallic conduction mechanism of scale-up continuous carbon nanotube sheets by mechanical stretching and stable chemical doping, Carbon 125 (2017) 649–658, https://doi.org/10.1016/j.carbon.2017.09.089.
[33] J.G. Park, Q. Cheng, J. Lu, J. Bao, S. Li, Y. Tian, Z. Liang, C. Zhang, B. Wang, Thermal conductivity of MWCNT/epoxy composites: the effects of length, alignment and functionalization, Carbon 50 (2012) 2083–2090, https://doi.org/10.1016/j.carbon.2011.12.046.
[34] A. Oluwalowo, N. Nguyen, S. Zhang, J.G. Park, R. Liang, Electrical and thermal conductivity improvement of carbon nanotube and silver composites, Carbon 146 (2019) 224–231, https://doi.org/10.1016/j.carbon.2019.01.073.
[35] B. Li, Y. Feng, G. Qian, J. Zhang, Z. Zhuang, X. Wang, The effect of gamma ray irradiation on PAN-based intermediate modulus carbon fibers, J. Nucl. Mater. 443 (2013) 26–31, https://doi.org/10.1016/j.jnucmat.2013.06.049.
[36] Y.Z. Wan, Y.L. Wang, Y. Huang, H.L. Luo, G.C. Chen, C.D. Yuan, Effect of surface treatment of carbon fibers with gamma-ray radiation on mechanical performance of their composites, J. Mater. Sci. 40 (2005) 3355–3359.
[37] I. Velo-Gala, J.J. López-Peñalver, M. Sánchez-Polo, J. Rivera-Utrilla, Surface modifications of activated carbon by gamma irradiation, Carbon 67 (2014) 236–249, https://doi.org/10.1016/j.carbon.2013.09.087.
[38] J. Guo, Y. Li, S. Wu, W. Li, The effects of γ-irradiation dose on chemical modification of multi-walled carbon nanotubes, Nanotechnology 16 (2005) 2385–2388, https://doi.org/10.1088/0957-4484/16/10/065.
[39] B. Hourahine, B. Aradi, V. Blum, F. Bonafé, A. Buccheri, C. Camacho, C. Cevallos, M.Y. Deshaye, T. Dumitric, A. Dominguez, S. Ehlert, M. Elstner, T. van der Heide, J. Hermann, S. Irle, J.J. Kranz, C. Köhler, T. Kowalczyk, T. Kubař, I.S. Lee, V. Lutsker, R.J. Maurer, S.K. Min, I. Mitchell, C. Negre, T.A. Niehaus, A.M. N. Niklasson, A.J. Page, A. Pecchia, G. Penazzi, M.P. Persson, J. Řezáč, C. G. Sánchez, M. Sternberg, M. Stöhr, F. Stuckenberg, A. Tkatchenko, V.W.Z. Yu, T. Frauenheim, DFTB+, a software package for efficient approximate density functional theory based atomistic simulations, J. Chem. Phys. 152 (2020), 124101, https://doi.org/10.1063/1.5143190.
[40] I. Ostanin, R. Ballarini, T. Dumitricə, Distinct element method for multiscale modeling of cross-linked carbon nanotube bundles: from soft to strong nanomaterials, J. Mater. Res. 30 (2014) 19–25, https://doi.org/10.1557/jmr.2014.279.
[41] R.H. Telling, C.P. Ewels, A.A. El-Barbary, M.I. Heggie, Wigner defects bridge the graphite gap, Nat. Mater. 2 (2003) 333–337, https://doi.org/10.1038/nmat876.
[42] H. Xu, J. Al-Ghalith, T. Dumitrică, Smooth sliding and superlubricity in the nanofriction of collapsed carbon nanotubes, Carbon 134 (2018) 531–535, https://doi.org/10.1016/j.carbon.2018.04.011.
[43] H. Xu, G. Drozdov, J.G. Park, B.D. Jensen, K.E. Wise, Z. Liang, G.M. Odegard, E. J. Siochi, T. Dumitrică, Computationally guided Design of large-diameter carbon nanotube bundles for high-strength materials, ACS Appl. Nano Mater. 4 (2021) 11115–11125, https://doi.org/10.1021/acsanm.1c02582.
[44] J.A. Kim, D.G. Seong, T.J. Kang, J.R. Youn, Effects of surface modification on rheological and mechanical properties of CNT/epoxy composites, Carbon 44 (2006) 1898–1905, https://doi.org/10.1016/j.carbon.2006.02.026.
[45] A.S. Krieg, J.A. King, G.M. Odegard, T.R. Leftwich, L.K. Odegard, P.D. Fraley, I. Miskioglu, C. Jolowsky, M. Lundblad, J.G. Park, R. Liang, Mechanical properties and characterization of epoxy composites containing highly entangled as-received and acid treated carbon nanotubes, Nanomaterials 11 (2021) 2445, https://doi.org/10.3390/nano11092445.
[46] M. Miyama, Y. Yang, T. Yasuda, T. Okuno, H.K. Yasuda, Static and dynamic contact angles of water on polymeric surfaces introduction and background information, Langmuir 13 (1997) 5494–5503, https://doi.org/10.1021/la960870n.
[47] C.P. Liu, P. Saha, Y. Huang, S. Shimpalee, P. Satjaritanun, I.V. Zenyuk, Measurement of contact angles at carbon fiber-water-air triple-phase boundaries inside gas diffusion layers using X-ray computed tomography, ACS Appl. Mater. Interfaces 13 (2021) 20002–20013, https://doi.org/10.1021/acsami.1c00849.
[48] L. He, A. Karumuri, S.M. Mukhopadhyay, Wettability tailoring of nanotube carpets: morphology-chemistry synergy for hydrophobic-hydrophilic cycling, RSC Adv. 7 (2017) 25265–25275, https://doi.org/10.1039/c7ra02745a.
[49] L. Zhang, J. Wang, C.A. Fuentes, D. Zhang, A.W. van Vuure, J.W. Seo, D. Seveno, Wettability of carbon nanotube fibers, Carbon 122 (2017) 128–140, https://doi.org/10.1016/j.carbon.2017.06.027.